

Photon-mediated Stroboscopic Quantum Simulation of a \mathbb{Z}_2 Lattice Gauge Theory

Tsafrir Armon and Shachar Ashkenazi

Racah Institute of Physics, Hebrew University of Jerusalem, Jerusalem 91904, Israel

Gerardo García-Moreno

Institute of Fundamental Physics IFF-CSIC, Calle Serrano 113b, 28006 Madrid, Spain
Departamento de Física Teórica and IPARCOS, Universidad Complutense de Madrid, 28040 Madrid, Spain and
Instituto de Astrofísica de Andalucía (IAA-CSIC),
Glorieta de la Astronomía, 18008 Granada, Spain

Alejandro González-Tudela*

Institute of Fundamental Physics IFF-CSIC, Calle Serrano 113b, 28006 Madrid, Spain

Erez Zohar[†]

Racah Institute of Physics, Hebrew University of Jerusalem, Jerusalem 91904, Israel

Quantum simulation of lattice gauge theories (LGTs), aiming at tackling non-perturbative particle and condensed matter physics, has recently received a lot of interest and attention, resulting in many theoretical proposals, as well as several experimental implementations. One of the current challenges is to go beyond 1+1 dimensions, where four-body (plaquette) interactions, not contained naturally in quantum simulating devices, appear. In this Letter, we propose a method to obtain them based on a combination of stroboscopic optical atomic control and the non-local photon-mediated interactions appearing in nanophotonic or cavity QED setups. We illustrate the method for a \mathbb{Z}_2 lattice Gauge theory. We also show how to prepare the ground state and measure Wilson loops using state-of-the-art techniques in atomic physics.

Gauge theories are so fundamental in both particle and condensed matter physics, that it almost seems redundant to explain why: with their local symmetries, they offer a consistent way to mediate interactions between matter particles, carried by gauge bosons. In spite of their clear description of fundamental forces, such as those of the standard model, many important phenomena in such models are still hidden behind the non-perturbative curtain. LGTs [1, 2] have been an important tool for tackling with such problems: combined with Monte-Carlo methods, they have enabled to compute an enormous amount of valuable physical data (e.g. the hadronic spectrum [3]). While these computations are useful and widely applicable to a variety of important physical problems, they cannot deal with real time evolution (since they are performed in a Euclidean spacetime) or with important scenarios with finite chemical potential, due to the sign problem [4].

To circumvent these limitations, quantum simulators of LGTs [5–9] based on cold atoms in optical lattices [10–29], trapped ions [30–33], superconducting qubits [34–37], and Rydberg atoms [38–42] have been proposed. These theoretical efforts have already culminated in several experimental realizations [43–47], benchmarking the validity and applicability of the quantum simulation method (as well as quantum computing methods [48–53]). Yet, so far, the experimental implementations have been limited to one-dimensional and/or small systems. One of the current challenges of the field is thus precisely to simulate LGTs in more than $1 + 1d$. Such sim-

ulations are especially hard [54] due to the four-body interactions associated with the magnetic plaquette interactions they involve [55]. The analog proposals to which were based on perturbative constructions, either by enforcing the symmetries [10] or using gauge invariant building blocks [13], which made the available plaquette interactions very weak. A way to avoid that is to implement the dynamics stroboscopically, such that two-body interactions with ancillary degrees of freedom yield the desired four-body interactions [20, 21, 39, 40, 56]. However, despite the many advantages of this approach, if the ancilla-system interaction is local, sequential actions are required for creating the plaquette interactions, each with an interaction of one of the four participating degrees of freedom with the ancilla alone, wasting precious experimental coherence time. For example, this is the case of Refs. [20, 21] where the two-body interactions are obtained by adiabatically moving atoms and relying on their collision - a very slow process.

In this Letter, we propose an alternative stroboscopic strategy to obtain such four-body interactions using the non-local, tunable, photon-mediated interactions which appear naturally when placing atoms close to photonic crystals [57–70] or within cavity mirrors [71–74]. In particular, by using a judicious combination of magnetic field gradients and time-modulated Raman transitions [60, 72–74], we will be able to entangle an ancilla array to all the plaquette atoms *simultaneously* and avoid the sequential nature of previous proposals [20, 21]. Such simultaneous action was also proposed in the toric code

simulation of [56] and the $U(1)$ proposal of [75] using Rydberg excited states with finite lifetimes. In our case, the physical degrees are encoded in metastable atomic states, and we use Raman photon-assisted transitions to make them interact. With that tool, we discuss in detail a method to simulate a pure \mathbb{Z}_2 LGT in $2+1d$. Besides, we also show how one can adiabatically find the model's ground state, and measure important properties, such as Wilson loops, using state-of-the-art AMO techniques.

\mathbb{Z}_2 Lattice Gauge Theory. The interest in \mathbb{Z}_N LGTs [76] is twofold. First, their large N limit reproduces compact QED ($U(1)$), and thus they can be used as consistent finite local Hilbert space approximations for studying it on quantum simulators. Second, \mathbb{Z}_N is the center of $SU(N)$, which makes \mathbb{Z}_N relevant for studying $SU(N)$ confinement [77]. Here we focus on the simplest case - \mathbb{Z}_2 [78]. Quantum simulations of \mathbb{Z}_N LGTs have been proposed [14, 20, 28, 79], and in particular for the \mathbb{Z}_2 case [20, 80–84]. The $1+1d$ case was implemented experimentally in Ref. [45].

The \mathbb{Z}_2 LGT is based on the algebra defined by two anticommuting operators which square to the identity, on local two dimensional spaces; e.g. the Pauli operators σ_x and σ_z . We place such a Hilbert space on each link of a two-dimensional lattice (blue spheres in Fig. 1(a)), and introduce the local gauge transformations acting on the four links around each site \mathbf{x} ,

$$A(\mathbf{x}) = \sigma_z(\mathbf{x}, 1) \sigma_z(\mathbf{x}, 2) \sigma_z(\mathbf{x} - \hat{1}, 1) \sigma_z(\mathbf{x} - \hat{2}, 2), \quad (1)$$

where the links are labelled by the pair $\mathbf{x}, k = 1, 2$ of their starting site and direction respectively. The dynamics is given by the Hamiltonian $H = H_E + H_B$ [76], where

$$H_E = -\lambda_E \sum_{\mathbf{x}, k} \sigma_z(\mathbf{x}, k), \quad (2)$$

is the electric Hamiltonian, and

$$H_B = -\lambda_B \sum_{\mathbf{x}} B(\mathbf{x}), \quad (3)$$

is the magnetic Hamiltonian, with $B(\mathbf{x}) = \sigma_x(\mathbf{x}, 1) \sigma_x(\mathbf{x} + \hat{1}, 2) \sigma_x(\mathbf{x} + \hat{2}, 1) \sigma_x(\mathbf{x}, 2)$. Note that $[A(\mathbf{x}), B(\mathbf{y})] = 0$ for any \mathbf{x}, \mathbf{y} , and thus $[H, A(\mathbf{x})] = 0$ for any \mathbf{x} , defining a local symmetry.

Stroboscopic Evolution. To mitigate the difficulty of creating the $H_E + H_B$ simultaneously, we turn to a stroboscopic evolution, given by the Trotter formula $e^{-iHt} = \lim_{M \rightarrow \infty} (e^{-iH_E t/M} e^{-iH_B t/M})^M$ [85, 86]. The challenge is to implement the unitary operators $e^{-iH_j t/M}$, within the simulator, especially H_B with its four-body interactions. Next, we will describe how this stroboscopic evolution was done in Refs. [20, 21], and show how to improve this protocol using tunable photon-mediated interactions.

The key idea of the method of Refs. [20, 21] is to introduce an array of auxiliary degrees of freedoms (controls)

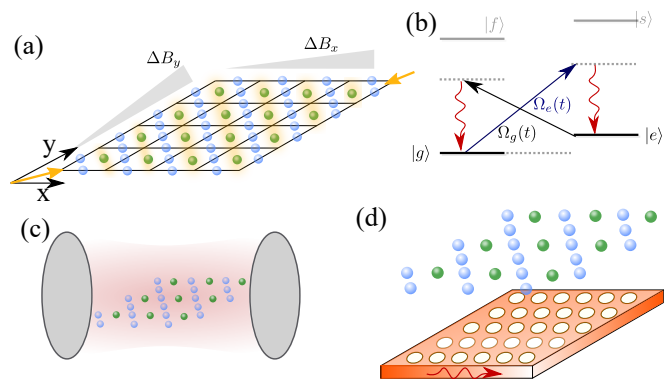


FIG. 1. (a) Scheme of the simulators: a two-dimensional array of atoms will play the role of the physical degrees of freedom along the links (in blue). Another two-dimensional array is interspersed such that one has an additional control atoms within the plaquettes (in green). Both the control/link atoms can be controlled independently by changing the relative phase of the lasers generating a diagonal standing wave (in orange). (b) Scheme of the atomic level structure: the \mathbb{Z}_2 Hilbert space of the simulator will be obtained with two atomic metastable states, g, e . We use Raman-photon assisted transitions in a butterfly configuration to induce and control the photon-mediated interactions. The photon field mediating the interactions can be either a cavity field (c) or the guided photons in 2D photonic crystals (d).

within the plaquettes (in green in Fig. 1(a)), with the same Hilbert space as on the links (two level systems in our case). The controls (whose operators and states will hereby be denoted with a $\tilde{\cdot}$) allow to convert the four-body interaction with a set of four two-body interactions between the control and the links around it. To do it, one creates *stators* [87, 88] using the unitary controlled operators:

$$\mathcal{U}_{\mathbf{x}}^{(i)} = \left| \tilde{\downarrow} \right\rangle \left\langle \tilde{\downarrow} \right|_{\mathbf{x}} + \sigma_x^{(i)} \left| \tilde{\uparrow} \right\rangle \left\langle \tilde{\uparrow} \right|_{\mathbf{x}}. \quad (4)$$

acting on the control of plaquette whose lower left corner is \mathbf{x} and a link i of the same plaquette. The controls are initialized to $|\tilde{i}n\rangle = \left(\left| \tilde{\uparrow} \right\rangle + \left| \tilde{\downarrow} \right\rangle \right) / \sqrt{2}$, and the action of $\mathcal{U}_{\mathbf{x}}^{(i)}$ results in the stator $S_{\mathbf{x}}^{(i)} = \mathcal{U}_{\mathbf{x}}^{(i)} |\tilde{i}n\rangle_{\mathbf{x}}$ which, maps states of the physical system (links) to states in the product space of links and controls. $S_{\mathbf{x}}^{(i)}$ obeys $\tilde{\sigma}_x(\mathbf{x}) S_{\mathbf{x}}^{(i)} = S_{\mathbf{x}}^{(i)} \sigma_x^{(i)}$ - allowing one to trade operations on the links with operations on the controls. Labeling the links in the plaquette by $i = 1 \dots 4$ (the order is irrelevant since \mathbb{Z}_2 is Abelian), the process could be repeated for all links in the plaquette, to obtain $S_{\mathbf{x}} = \mathcal{U}_{\mathbf{x}}^{(1)} \mathcal{U}_{\mathbf{x}}^{(2)} \mathcal{U}_{\mathbf{x}}^{(3)} \mathcal{U}_{\mathbf{x}}^{(4)} |\tilde{i}n\rangle_{\mathbf{x}}$, for which $\tilde{\sigma}_x(\mathbf{x}) S_{\mathbf{x}} = S_{\mathbf{x}} B(\mathbf{x})$. The operators $\mathcal{U}_{\mathbf{x}}^{(i)}$ commute, and thus they could also be applied simultaneously, if the simulating system allows for it (which was not the case of the previous cold atom proposals [20, 21]). The trotterization errors [89] of the scheme have been studied in [20, 25], and importantly, since each step is invariant

on its own, the gauge symmetry is not violated. The exact form of $\mathcal{U} = \prod_{\mathbf{x}} \prod_{i \in p(\mathbf{x})} \mathcal{U}_{\mathbf{x}}^{(i)}$ (where $p(\mathbf{x})$ is the plaquette whose lower left corner is \mathbf{x} and i labels its four links, in a counter-clockwise order from \mathbf{x}) is given in the Supplemental Material. The main requirements from our simulator are thus (R1) to have separate control on the links and the controls; and (R2) to allow nearest neighbor control-link interactions of the form $\sigma_{x(z)} \tilde{\sigma}_{x(z)}$.

Photon-mediated LGT simulator. The different elements of the simulator we propose are sketched in Fig. 1. The basis is to have a two-dimensional ordered array of ultra-cold atoms as depicted in Fig. 1(a) which can be obtained either with optical lattices [90] or with the latest advances in optical tweezer techniques [91–93]. In contrast to other proposals, we assume the atoms do not move, and the interactions among them will be obtained through the exchange of photons. To control these photon mediated interactions the atoms are assumed to have a level structure as depicted in Fig. 1(b). The ground states, $|g\rangle$ and $|e\rangle$, will define the two level system we need, whereas the optically excited states $|f\rangle$ and $|s\rangle$ will be used for inducing Raman-assisted transitions between the control/link atoms either by coupling them to cavity photons, Fig. 1(c), or to the guided modes propagating within a photonic crystal, see Fig. 1(d). Individual rotations of each control/link degree of freedom can be obtained with two-photon Raman transitions via the same or another excited state. Let us now see in detail how these platforms can potentially fulfill all the required ingredients for the simulators.

Note that if we label as a the optical lattice constant, using two counter-propagating beams with in-plane wave number of $\mathbf{k}_{xy} = \pm(\pi/2a)(\hat{x} + \hat{y})$ and phase difference of ϕ , one can address only the controls (links) by switching $\phi = 0$ (π), as schematically depicted in orange in Fig. 1(a). Another more demanding alternative consists of using quantum gas microscopes [94–96], which have already enabled single-site imaging/addressing. In any case, the first requirement (R1) can thus be satisfied. Let us now go to the non-trivial part of tailoring the two-body interactions between the plaquette and controls. Since the atoms are fixed in our implementation, as compared to Refs. [20, 21], we will use the non-local interactions that are induced by the exchange of photons through their optical transition [60, 72–74]. As explained in Refs. [58, 60], by choosing a *butterfly* Raman configuration as depicted in Fig. 1(b), with equal Raman weight $\frac{|\Omega_e|^2}{\Delta_e} = \frac{|\Omega_g|^2}{\Delta_g} \equiv R$, and tuning the effective frequency of the Raman transition far from the cavity frequency or within a band-gap in the cavity/photonic crystal implementations, respectively, one can arrive to the following effective interactions between atoms

$$H_{\text{eff}} = J \sum_{j,l} \sigma_x^j \sigma_x^l f(\mathbf{r}_j - \mathbf{r}_l). \quad (5)$$

Here, J is the overall spin-spin interaction strength, which is proportional to R , such that the interactions can be switched on and off through the Raman lasers Ω_i , and to the atom-cavity/nanophotonic coupling strength. One advantage of the nanophotonic platform is that thanks to the confinement of light, J can potentially be of the order of GHz [58, 70], that could make the simulation considerably faster than other systems. The spatial dependence of the interactions is encoded in $f(\mathbf{r}_j - \mathbf{r}_l)$ and depends on the particular implementation chosen. For cavity QED setups, the interactions are infinite range $|f(\mathbf{r}_i - \mathbf{r}_j)| \approx 1$, such that *all* atoms will interact if they are not placed in nodes of the cavity mode. In two-dimensional nanophotonic waveguides [60, 97], the interactions are mediated by an atom-photon bound-state which yields $|f(\mathbf{r}_i - \mathbf{r}_j)| \propto e^{-|\mathbf{r}_{ij}|/L} / \sqrt{|\mathbf{r}_{ij}|/L}$, with a tunable L through the system parameters, such as the Raman laser frequency ω_L . Note that in neither case the interactions takes the desired nearest-neighbour form required for the simulation (R2). In the nanophotonic case, one can approximately obtain it by making $L \sim a$. However, the residual couplings to other neighbours break the Gauge symmetry and spoil the simulation (See Sup. Material for details). The way to circumvent this problem was proposed in Ref. [60], and already experimentally implemented in cavity QED setups [72–74]: it consists of a combination of magnetic field gradients along the X and Y direction, so that each photon-mediated transitions at a given distance has a different resonance, plus time-modulated Raman transitions $\Omega_i(t) = \sum_{\alpha} \bar{\Omega}_{\alpha} e^{i\bar{\omega}_{\alpha} t}$, where $\bar{\omega}_{\alpha}$ is the detuning from the main laser frequency ω_L . Thus, choosing adequately $(\bar{\Omega}_{\alpha}, \bar{\omega}_{\alpha})$ one can design any spatial interaction pattern allowed by $f(\mathbf{r}_i - \mathbf{r}_j)$. Concretely, for a magnetic gradient $B = \nabla B(p\hat{x} + q\hat{y})$, a Zeeman splitting would be induced at site m with position (x^m, y^m) such that $\omega_e^{(m)} = \mu_B \nabla B(p x^m + q y^m)$. This leads to a different Raman condition for the interaction between each pair of sites that reads $\bar{\omega}_{\alpha} - \omega_e^{(m)} = \bar{\omega}_{\beta} - \omega_e^{(n)}$, which for the desired nearest-neighbors interactions would reduce to $\bar{\omega}_{\alpha} - \bar{\omega}_{\beta} = \mu_B \nabla B p$ or $\mu_B \nabla B q$, for the horizontal and vertical hoppings, respectively. Here p, q can be, for example, two incommensurable irrational numbers such that the energy difference of vertically or horizontally adjacent sites can not repeat at any other distance. Therefore, only two sidebands $\bar{\omega}_{\alpha}$ would be needed to match the nearest neighbour in the vertical and horizontal directions. The interactions among the different neighbours would then be suppressed because every other pair of non-nearest-neighbor sites has different energy difference from the ones included in the time-modulated Raman fields.

Apart from these Gauge breaking terms, another potential source of error in the simulation introduced by such photon-mediated interactions is the finite lifetime of the cavity/photonic crystal photons. The effect of these

losses in the fidelity of the entangling gates has been well-characterized [58], and scale with $1 - F \propto 1/\sqrt{C}$, with C being the cooperativity factor of the system. Recent experiments have already reached values $C \sim 5-30$ [70, 74], although values of $C \sim 10^4$ are feasible with fabrication and trapping improvements [58].

Simulation Step — With the photon-mediated interactions at hand, we can prescribe a single first order trotter step. It is given by

$$W_E(t_0, \tau) W_B(t_0, \tau), \quad (6)$$

where t_0 is the the time step's beginning, and τ is its duration. The electric and magnetic steps are given by $W_i = \exp[-i\tau H_i(t_0 + \tau/2)]$. The electric term is easily created by a single body operation on the links, $W_E(t_0, \tau) = V_z(\tau\lambda_E(t_0 + \tau/2))$. Here we designate single body operations on the links as $V_i(\Phi) = \exp(i\Phi \sum_j \sigma_i^j)$ and similarly $\tilde{V}_i(\Phi)$ for the controls. As described above, the magnetic term is realized by creating the stators on every plaquette simultaneously, applying the operation on the controls, and undoing the stators, or

$$W_B(t_0, \tau) = \mathcal{U}^\dagger \tilde{V}_x(\tau\lambda_B(t_0 + \tau/2)) \mathcal{U}, \quad (7)$$

where \mathcal{U} is the stator creation operator, whose the exact form is given in the Supplemental Material. The operator \mathcal{U} relies on single-body operations as well as two-body nearest neighbors interactions for which one uses H_{eff} ((5)) along with the magnetic field gradient. Unlike previous proposals [20, 21], here \mathcal{U} is implemented simultaneously on all plaquettes and links. It should be noted that a second order trotterization [98] could be used without adding applications of W_B . Because the atom-atom interactions in W_B are the main experimental bottle-neck (in terms of fidelity), such second order should be favorable.

Adiabatic Evolution — As an example for the dynamics that could be simulated with our proposed scheme, we examine adiabatic ground state preparation. Such a process should be done with caution, as the \mathbb{Z}_2 theory has a phase transition [99] where the gap vanishes and the adiabatic theorem cannot be used. We show, however, that it is possible to perform the procedure from both sides of the phase transition, such that one can choose the correct side according to the desired values of $\lambda_{E,B}$, without ever crossing the transition. Various numerical and renormalization schemes put the transition slightly over $\lambda_B/\lambda_E \approx 3$ [100–102].

The straightforward direction of the two, is to start with $\lambda_B = 0$, and set the initial state of the links to the ground state of H_E . This ground state is trivial, and easy to initialize because it involves only single-atom operations: each link should be prepared in the spin up state. Then, the simulation could be carried out, adiabatically increasing λ_B over time. The logic remains the same for

the second direction for which we start with $\lambda_E = 0$ and initialize the system in the ground state of the magnetic Hamiltonian. However, initializing this ground state is not as trivial. To do it one can use \mathcal{U} and post-selection projection, as demonstrated below. As shown in the supplemental material, the sequence

$$\tilde{\Pi}_x \mathcal{U} |\phi_0\rangle \otimes |\tilde{i}n\rangle \quad (8)$$

where $|\phi_0\rangle = \otimes_{\text{links}} |\uparrow\rangle$ and $\tilde{\Pi}_x$ is a projection operator onto the "up" eigenstates of $\tilde{\sigma}_x$ of all the controls yields the ground state of the system (known as the toric code ground state [103]). Such a projection operator could be realized e.g. by rotating the controls to the x basis and then applying a $\pi/2$ pulse driving $|g\rangle \leftrightarrow |f_3\rangle$ to another excited state f_3 which is then allowed to emit to the environment. With the initial ground state in hand, the simulation could proceed by increasing λ_E over time.

Measurement — Upon achieving the final state, one can use the same tools to perform key measurements about the final state of the system. The relevant (gauge invariant) operators in this case are either local σ_z operators on the link, or the nonlocal Wilson loops, which serve as a probe for confinement [1]. In our case, they will be products of σ_x operators on closed paths. It was shown that the stator mechanism could be used to measure Wilson loops, even in a parallel fashion. The procedure is rather simple [104]: the control is initiated in the state $|\tilde{i}n\rangle$ and then undergoes a series of unitary operations similar to the ones introduced above with each of the links along the loop, thus creating a stator involving the control and all the links. At this point the Wilson loop data is stored in the control and it could be measured locally there. The simulator discussed here can perform many of the needed operations simultaneously, and even prepare all Wilson loops of the same size simultaneously (for more details on the implementation see Supplemental Material).

Numerical Simulations — To demonstrate the adiabatic preparation of the ground state, and possible measurement results, we now turn to numerical simulations of a lattice of size 4×4 plaquettes. The ratio λ_B/λ_E is increased or decreased linearly over time to accommodate the two adiabatic processes described above. To keep the simulations comparable (energy scale, frequencies etc.) when starting from the electric ground state the simulated Hamiltonian is $H = H_E + (\lambda_B/\lambda_E) H_B$, while when starting from the magnetic ground state the simulated Hamiltonian is taken as $H = (\lambda_E/\lambda_B) H_E + H_B$. We examine the expectation value $\langle \mathcal{W} \rangle$ of a Wilson loop of size 1×1 in the center of lattice, to minimize edge effects, which are dominant in such a small system. Figure 2 shows the expectation value $\langle \mathcal{W} \rangle$ for the adiabatically prepared ground states as function of the final ratio λ_B/λ_E for the two preparation directions. One can see that the simulations agree with the exact ground state in

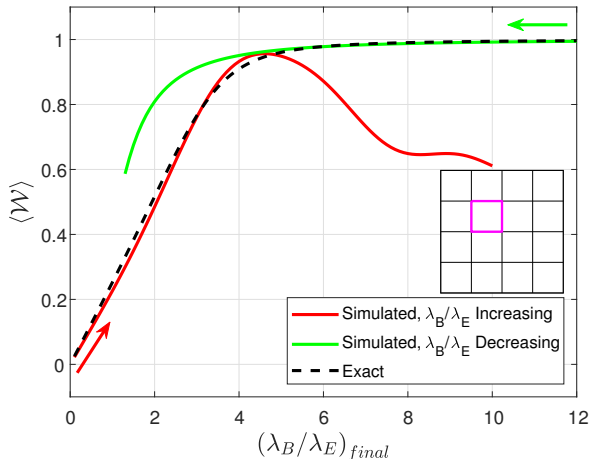


FIG. 2. The expectation value $\langle \mathcal{W} \rangle$ for a Wilson loop of size 1×1 in the bulk of a lattice of size 4×4 plaquettes, as function of the final ratio λ_B/λ_E , following an adiabatic preparation of the ground state (see main text). The red (green) line shows $\langle \mathcal{W} \rangle$ for the adiabatically prepared ground state when λ_B/λ_E increases (decreases) with time (The colored arrows mark the direction of λ_B/λ_E change over time). The dashed black line shows $\langle \mathcal{W} \rangle$ for the exact ground state. The total simulation time is 1 and the number of trotter steps is 80. The inset shows the 4×4 lattice with the Wilson loop highlighted in magenta.

their respective sides. Due to the small size of the system, this crossing is not directly related to the phase transition which appears in the thermodynamic limit, but nonetheless demonstrates the advantages of our proposed method since for the same number of trotter steps, better fidelity is achieved by selecting the evolution direction of λ_B/λ_E , even in the absence of a phase transition (for more details see Supplemental Material). Even in the thermodynamic limit, for every value of λ_B/λ_E , except values close to the phase transition, it is possible to adiabatically prepare the ground state by a proper choice of the evolution direction in λ_B/λ_E . Furthermore, by experimentally measuring $\langle \mathcal{W} \rangle$ from both sides, the phase transition itself could be identified by looking for the crossing of the two measurements.

To conclude, we have shown how to use the non-local photon-mediated interactions appearing in cavity and nanophotonic setups to implement a Z_2 LGT simulator. In particular, we demonstrate how the possibility of inducing multi-qubit gates between the ancillary and the physical degrees of freedom allows us to simplify the stroboscopic stator protocol developed in Refs. [20, 21]. The stator procedure can be generalized in a straightforward fashion to any gauge group [21], but when the group is non-Abelian a sequential action is necessary for generating the plaquettes, due to the group's non-commutativity. The procedure shown here can hence be generalized for studying further Z_N LGTs, also as

a method to approximate $U(1)$ physics. It can also be generalized to include dynamical matter. The ideas introduced in this letter could obviously be adapted in a straightforward manner for the toric code implementation (by adding more controls on the sites, and replacing H_E by $H_A = -\lambda_A \sum_{\mathbf{x}} A(\mathbf{x})$).

Acknowledgments — We would like to thank A. Sterdyniak for fruitful discussions. EZ acknowledges support by the Israel Science Foundation (grant No. 523/20). AGT acknowledges support from CSIC Research Platform on Quantum Technologies PTI-001 and from Spanish project PGC2018-094792-B-100(MCIU/AEI/FEDER, EU). GGM acknowledges financial support from the GEFES prize, State Agency for Research of the Spanish MCIU through the “Center of Excellence Severo Ochoa” award to the Instituto de Astrofísica de Andalucía (SEV-2017-0709), from IPARCOS (Instituto de Física de Partículas y el Cosmos) and from the Spanish Government through the project PID2019-107847RB-C44.

SUPPLEMENTAL MATERIAL

CREATING THE SIMULATION STEP

The simulating system allows one to create single site operations on the links or the controls which we designate by $V_i(\phi) = \exp(-i\phi \sum_j \sigma_i^j)$ where $i = x, y, z$ and the summation is over all links, or all controls for $\tilde{V}_i(\phi)$. This allows for the creation of the electric Hamiltonian and the electric portion of the time step via $W_E(t_0, \tau) = V_z(-\tau\lambda_E[t_0])$.

To create the magnetic Hamiltonian and the magnetic portion of the time step, one needs to create the stator by applying $\mathcal{U} = \prod_{\mathbf{x}} \prod_{i \in p(\mathbf{x})} \mathcal{U}_{\mathbf{x}}^{(i)}$ where the first (second) product is over all plaquettes (links around the plaquette). $\mathcal{U}_{\mathbf{x}}^{(i)}$ is given by $\exp(-i\frac{\pi}{4}\tilde{\sigma}_z(\mathbf{x})\sigma_x^{(i)})\exp(-i\frac{\pi}{4}\sigma_x^{(i)})\exp(-i\frac{\pi}{4}\tilde{\sigma}_z(\mathbf{x}))$ but because many of the operators commute and could be carried out simultaneously, in terms of the control operations available in the simulating system, \mathcal{U} is simply carried out as

$$\mathcal{U} = \left[\tilde{V}_y\left(\frac{\pi}{4}\right) \right]^\dagger V_I \tilde{V}_y\left(\frac{\pi}{4}\right) V_x\left(\frac{\pi}{4}\right). \quad (9)$$

Here $V_I = \exp(-i\frac{\pi}{4}\sum_{(i,j)}\sigma_x^i\tilde{\sigma}_x^j)$ where the summation is over all nearest-neighbors control-link pairs. V_I is created by applying Hamiltonian (5) for the appropriate duration. The unitaries \tilde{V}_y in Eq. (9) serve to transform $\tilde{\sigma}_x$ in V_I to $\tilde{\sigma}_z$ to allow for the creation of the stator.

Then a single trotter step [Eq. (6)] could be expressed

as follows:

$$\begin{aligned} W_E(t_0, \tau) &= V_z(-\tau\lambda_E[t_0]), \\ W_B(t_0, \tau) &= \mathcal{U}^\dagger \tilde{V}_x(-\tau\lambda_B[t_0]) \mathcal{U}, \end{aligned} \quad (10)$$

UNDESIRE INTERACTIONS

Our proposal calls for two-body nearest neighbors interaction, via the use of a tailored magnetic gradient and driving field. It is nonetheless interesting to examine the effects of undesired interactions of atoms further apart from each other. Suppose we include in the interaction term V_I other pairs of atoms than the nearest neighbors, the added terms could be split into three categories - link-link interactions, control-control interactions and control-link interactions.

Undesired link-link interactions in V_I will have the form $\sigma_x^i \sigma_x^j$, and will thus commute with every other term in W_B (which for the links only involves σ_x). Therefore, within a single time step, the application of \mathcal{U} and \mathcal{U}^\dagger will cancel out the effects of all such undesired interactions. Undesired control-control interactions, however, do not commute with W_B , but they do cancel out almost entirely for consecutive time steps. If we designate $\mathcal{U}_{\text{actual}} = \mathcal{U}\mathcal{U}_{\text{CC}}$ where \mathcal{U}_{CC} is the contribution of the undesired control-control interactions, such that $[\mathcal{U}, \mathcal{U}_{\text{CC}}] = 0$, \mathcal{U}_{CC} involves only the controls and thus commutes with W_E . Therefore, a single time step could be written as:

$$\mathcal{U}_{\text{CC}}^\dagger W_E(t_0, \tau) W_B(t_0, \tau) \mathcal{U}_{\text{CC}}, \quad (11)$$

and therefore, following consecutive time steps \mathcal{U}_{CC} will cancel out except for \mathcal{U}_{CC} ($\mathcal{U}_{\text{CC}}^\dagger$) in the first (last time step). Thus, it will be possible to cancel out all control-control undesired interactions with two applications of two-body interactions targeted only at the controls. This could be done in a similar fashion to the proposed single-body operations only on the controls or the links.

The last group includes undesired control-link interactions. This group is the most problematic one, as it doesn't commute with W_B or W_E , and can not be readily canceled out. Furthermore, these interactions break the gauge symmetry. It should be noted that in the context of photonic waveguide with its spatially declining coupling, the undesired interactions are exponentially suppressed, with the shortest undesired control-link interaction $\sqrt{5}$ times larger than the desired interaction distance. If this suppression is not sufficient, one can split the lattice into sublattices which will be addressed sequentially, such that atoms with undesired couplings will be even further apart.

ADIABATIC EVOLUTION IN A (SMALL) FINITE SIZE SYSTEM

The Z_2 LGT exhibits a phase transition in the thermodynamic limit ($N \rightarrow \infty$ for system of size $N \times N$ plaquettes), but naturally, any experiment will be carried out with a finite size system, and our simulations are limited to small systems (up to 4×4 plaquettes). While the energy gap for finite systems does not vanish like in the thermodynamic limit, the gap decreases with system size and also depends on the ratio λ_B/λ_E . Therefore, even though small systems do not exhibit the phase transition, the decreasing energy gap recreates some of the difficulties posed by the phase transition, due to the adiabaticity demands. The smaller the energy gap, the longer the process must be to obey the adiabaticity condition [105], and more trotter steps will be needed. Thus, even for a finite (and even small) system it is hard (though not impossible) to adiabatically prepare the ground state for every value λ_B/λ_E when starting from either side of the λ_B/λ_E axis. Even though our numerical simulations do not exhibit the expected phase transition of the thermodynamic limit, they still demonstrate how choosing the evolution direction in λ_B/λ_E can improve the fidelity of the process, without extending the process duration and adding more trotter steps.

Figure (3) shows similar results to those of Fig. (2) for a 1×1 Wilson loop in the center of a 3×3 array. However, the duration of the process is increased from the top panel to the bottom one. One can observe that as the duration of the process increases the two directions of preparation better agree with the exact result - as a result of the increased adiabaticity. However, by choosing the appropriate direction one can reach the desired fidelity with shorter duration (and less trotter steps). This effect will not be possible in the thermodynamic limit where the vanishing energy gap will not allow for adiabatic preparation beyond the phase transition (no matter the duration of the process).

INITIALIZING H_B GROUND STATE

One can easily verify that the ground state of $-H_B$ is given by

$$|0\rangle = \prod_{\mathbf{x}} \left(\frac{1 + \prod_{i \in p(\mathbf{x})} \sigma_x^i}{2} \right) |\phi_0\rangle, \quad (12)$$

where the outer product is over all plaquettes, the inner product is over all links in that plaquette and $|\phi_0\rangle = (\otimes_{\text{links}} |\uparrow\rangle)$. To initialize the ground state, we note that for $|\Psi\rangle = |\phi_0\rangle \otimes |\tilde{n}\rangle$ one has

$$\mathcal{U}|\Psi\rangle = \prod_{\mathbf{x}} \left(\frac{1}{\sqrt{2}} |\tilde{\uparrow}\rangle_{\mathbf{x}} + \frac{1}{\sqrt{2}} |\tilde{\downarrow}\rangle_{\mathbf{x}} \prod_{i \in \mathbf{x}} \sigma_x^i \right) |\phi_0\rangle. \quad (13)$$

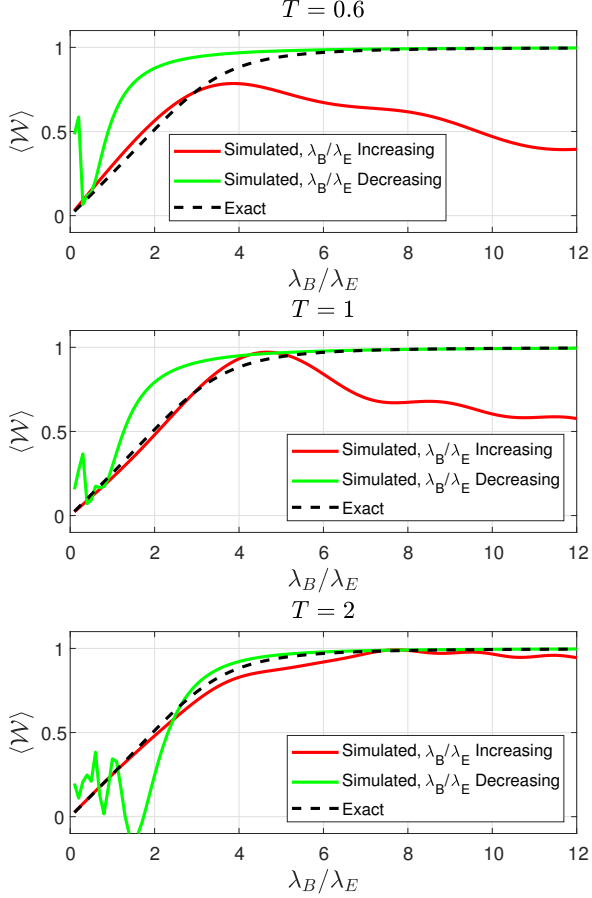


FIG. 3. Similar to Fig. (2) but for a 1×1 Wilson loop in the center of a 3×3 array. The duration T of the process is 0.6, 1, 2 for the top, middle and bottom panels respectively. The trotter step duration is kept the same so the number of trotter steps M scales with T and is 48, 80, 160 in the same order.

In terms of the eigenvectors along the x direction the term in the product reads

$$\left| \tilde{\uparrow}_x \right\rangle_x \otimes \frac{1 + \prod_{i \in x} \sigma_x^i}{2} + \left| \tilde{\downarrow}_x \right\rangle_x \otimes \frac{1 - \prod_{i \in x} \sigma_x^i}{2}, \quad (14)$$

and therefore

$$\tilde{\Pi}_x \mathcal{U} |\phi_0\rangle \otimes |\tilde{i}n\rangle = |0\rangle \otimes_{\text{controls}} \left| \tilde{\uparrow}_x \right\rangle \quad (15)$$

where $\tilde{\Pi}_x$ is a product of projection operators onto the "up" eigenstate of $\tilde{\sigma}_x$.

MEASUREMENT OF WILSON LOOPS

To measure a Wilson Loop, one must apply controlled unitaries to entangle the relevant control with each link

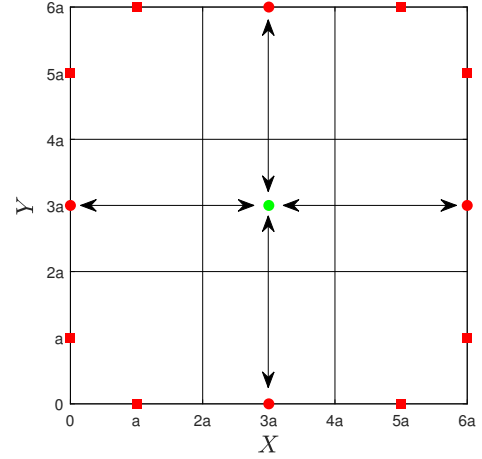


FIG. 4. The links (red) and control (green) involved in a 3×3 Wilson loop (other controls and links are omitted). The links are split into two sets of equal distance from the control (circles vs. squares). The arrows demonstrate the simultaneous application of the unitary on the first set.

along the loop, creating a stator. Unlike previous proposals where this process takes place sequentially, with the simulator discussed here, many steps could be performed simultaneously. First, we examine the loop and a control which is located at or near its center. Then, we divide the links into sets of identical distances from the control. The most efficient choice is a square loop of size $N \times N$ plaquettes with N odd. For this choice the control lies exactly at the center, thus minimizing the number of sets (this number scales linearly with N). For each set, the magnetic gradient and driving field must be adjusted to select its distance as the desired interaction distance (in a similar fashion to the choice of nearest-neighbor interactions before). It should be noted that in the case of photonic waveguides the interaction length L is tuneable and even long range interactions are feasible [58, 106]. An operator \mathcal{W} , analogous to \mathcal{U} introduced above but connecting only the control and links relevant for the Wilson loop should then be applied, creating the desired a stator. This will generally involve repeating the process for every set of links (with different distances from the control) until we yield the desired total stator, and the results could be measured on the control. Figure 4 presents the links (red) and the control (green) in a 3×3 Wilson loop. The links are split to only two sets of equal distance from the control (squares vs. circles in the figure). The stator creation could take place using only two steps - applying the procedure on all the links of one set (say the circles as exemplified by arrows in the figure) and then on all the links in the other set.

It should be noted that we are not limited to the measurement of a single Wilson loop. In fact, applying the steps presented here will create the stators for every Wil-

son loop of the desired size - simultaneously - each one encoded on the control which lies at its center. Thus, measurements could be taken more efficiently than in previous proposals.

-
- * a.gonzalez.tudela@csic.es
 † erez.zohar@mail.huji.ac.il
- [1] K. G. Wilson, *Phys. Rev. D* **10**, 2445 (1974).
 - [2] J. B. Kogut, *Rev. Mod. Phys.* **51**, 659 (1979).
 - [3] S. Aoki, Y. Aoki, D. Bećirević, T. Blum, G. Colangelo, S. Collins, M. Della Morte, P. Dimopoulos, S. Dürr, H. Fukaya, M. Golterman, S. Gottlieb, R. Gupta, S. Hashimoto, U. M. Heller, G. Herdoiza, R. Horsley, A. Jüttner, T. Kaneko, C. J. Lin, E. Lunghi, R. Mawhinney, A. Nicholson, T. Onogi, C. Pena, A. Portelli, A. Ramos, S. R. Sharpe, J. N. Simone, S. Simula, R. Sommer, R. Van de Water, A. Vladikas, U. Wenger, and H. Wittig, “FLAG Review 2019: Flavour Lattice Averaging Group (FLAG),” (2020).
 - [4] M. Troyer and U.-J. Wiese, *Phys. Rev. Lett.* **94**, 170201 (2005).
 - [5] U.-J. Wiese, *Annalen der Physik* **525**, 777 (2013).
 - [6] E. Zohar, J. Cirac, and B. Reznik, *Reports on Progress in Physics* **79**, 014401 (2016).
 - [7] M. Dalmonte and S. Montangero, *Contemporary Physics* **57**, 388 (2016).
 - [8] M. C. Bañuls, R. Blatt, J. Catani, A. Celi, J. I. Cirac, M. Dalmonte, L. Fallani, K. Jansen, M. Lewenstein, S. Montangero, C. A. Muschik, B. Reznik, E. Rico, L. Tagliacozzo, K. Van Acoleyen, F. Verstraete, U.-J. Wiese, M. Wingate, J. Zakrzewski, and P. Zoller, *The European Physical Journal D* **74**, 165 (2020).
 - [9] N. Klco, A. Roggero, and M. J. Savage, “Standard model physics and the digital quantum revolution: Thoughts about the interface,” (2021), [arXiv:2107.04769 \[quant-ph\]](https://arxiv.org/abs/2107.04769).
 - [10] E. Zohar and B. Reznik, *Phys. Rev. Lett.* **107**, 275301 (2011).
 - [11] D. Banerjee, M. Dalmonte, M. Müller, E. Rico, P. Stebler, U. J. Wiese, and P. Zoller, *Phys. Rev. Lett.* **109**, 175302 (2012).
 - [12] E. Zohar, J. I. Cirac, and B. Reznik, *Phys. Rev. Lett.* **109**, 125302 (2012).
 - [13] E. Zohar, J. I. Cirac, and B. Reznik, *Phys. Rev. Lett.* **110**, 055302 (2013).
 - [14] E. Zohar, J. I. Cirac, and B. Reznik, *Phys. Rev. A* **88**, 023617 (2013).
 - [15] E. Zohar, J. I. Cirac, and B. Reznik, *Phys. Rev. Lett.* **110**, 125304 (2013).
 - [16] D. Banerjee, M. Bögli, M. Dalmonte, E. Rico, P. Stebler, U. J. Wiese, and P. Zoller, *Phys. Rev. Lett.* **110**, 125303 (2013).
 - [17] K. Stannigel, P. Hauke, D. Marcos, M. Hafezi, S. Diehl, M. Dalmonte, and P. Zoller, *Phys. Rev. Lett.* **112**, 120406 (2013).
 - [18] A. Bazavov, Y. Meurice, S. W. Tsai, J. Unmuth-Yockey, and J. Zhang, *Phys. Rev. D* **92**, 076003 (2015).
 - [19] Y. Kuno, K. Kasamatsu, Y. Takahashi, I. Ichinose, and T. Matsui, *New Journal of Physics* **17**, 63005 (2015).
 - [20] E. Zohar, A. Farace, B. Reznik, and J. I. Cirac, *Physical Review Letters* **118** (2017), [10.1103/PhysRevLett.118.070501](https://doi.org/10.1103/PhysRevLett.118.070501).
 - [21] E. Zohar, A. Farace, B. Reznik, and J. Cirac, *Physical Review A* **95** (2017), [10.1103/PhysRevA.95.023604](https://doi.org/10.1103/PhysRevA.95.023604).
 - [22] V. Kasper, F. Hebenstreit, F. Jendrzejewski, M. K. Oberthaler, and J. Berges, *New Journal of Physics* **19**, 023030 (2017).
 - [23] O. Dutta, L. Tagliacozzo, M. Lewenstein, and J. Zakrzewski, *Phys. Rev. A* **95**, 053608 (2017).
 - [24] D. González-Cuadra, E. Zohar, and J. I. Cirac, *New Journal of Physics* **19**, 063038 (2017).
 - [25] J. Bender, E. Zohar, A. Farace, and J. I. Cirac, *New Journal of Physics* **20**, 93001 (2018).
 - [26] T. V. Zache, F. Hebenstreit, F. Jendrzejewski, M. K. Oberthaler, J. Berges, and P. Hauke, *Quantum Science and Technology* **3**, 034010 (2018).
 - [27] E. Rico, M. Dalmonte, P. Zoller, D. Banerjee, M. Bögli, P. Stebler, and U. J. Wiese, *Annals of Physics* **393**, 466 (2018).
 - [28] E. Ercolessi, P. Facchi, G. Magnifico, S. Pascazio, and F. V. Pepe, *Phys. Rev. D* **98**, 074503 (2018).
 - [29] G. Magnifico, D. Vodola, E. Ercolessi, S. P. Kumar, M. Müller, and A. Bermudez, *Phys. Rev. B* **100**, 115152 (2019).
 - [30] P. Hauke, D. Marcos, M. Dalmonte, and P. Zoller, *Phys. Rev. X* **3**, 041018 (2013).
 - [31] D. Yang, G. S. Giri, M. Johanning, C. Wunderlich, P. Zoller, and P. Hauke, *Phys. Rev. A* **94**, 052321 (2016).
 - [32] Z. Davoudi, M. Hafezi, C. Monroe, G. Pagano, A. Seif, and A. Shaw, *Phys. Rev. Res.* **2**, 23015 (2020).
 - [33] Z. Davoudi, N. M. Linke, and G. Pagano, “Toward simulating quantum field theories with controlled phonon dynamics: A hybrid analog-digital approach,” (2021), [arXiv:2104.09346 \[quant-ph\]](https://arxiv.org/abs/2104.09346).
 - [34] D. Marcos, P. Rabl, E. Rico, and P. Zoller, *Phys. Rev. Lett.* **111**, 110504 (2013).
 - [35] D. Marcos, P. Widmer, E. Rico, M. Hafezi, P. Rabl, U. J. Wiese, and P. Zoller, *Annals of Physics* **351**, 634 (2014).
 - [36] A. Mezzacapo, E. Rico, C. Sabín, I. L. Egusquiza, L. Lamata, and E. Solano, *Phys. Rev. Lett.* **115**, 240502 (2015).
 - [37] G. Romero, E. Solano, and L. Lamata, “Quantum simulations with circuit quantum electrodynamics,” in *Quantum Simulations with Photons and Polaritons: Merging Quantum Optics with Condensed Matter Physics*, edited by D. G. Angelakis (Springer International Publishing, Cham, 2017) pp. 153–180.
 - [38] H. Weimer, M. Müller, I. Lesanovsky, P. Zoller, and H. P. Büchler, *Nature Physics* (2010), [10.1038/nphys1614](https://doi.org/10.1038/nphys1614).
 - [39] L. Tagliacozzo, A. Celi, A. Zamora, and M. Lewenstein, *Annals of Physics* **330**, 160 (2013).
 - [40] L. Tagliacozzo, A. Celi, P. Orland, M. W. Mitchell, and M. Lewenstein, *Nature Communications* **4**, 2615 (2013).
 - [41] F. M. Surace, P. P. Mazza, G. Giudici, A. Lerosé, A. Gambassi, and M. Dalmonte, *Phys. Rev. X* **10**, 021041 (2020).
 - [42] A. Celi, B. Vermersch, O. Viyuela, H. Pichler, M. D. Lukin, and P. Zoller, *Phys. Rev. X* **10**, 021057 (2020).
 - [43] E. A. Martinez, C. A. Muschik, P. Schindler, D. Nigg, A. Erhard, M. Heyl, P. Hauke, M. Dalmonte, T. Monz, P. Zoller, and R. Blatt, *Nature* **534**, 516 (2016).

- [44] C. Kokail, C. Maier, R. van Bijnen, T. Brydges, M. K. Joshi, P. Jurcevic, C. A. Muschik, P. Silvi, R. Blatt, C. F. Roos, and P. Zoller, *Nature* **569**, 355 (2019).
- [45] C. Schweizer, F. Grusdt, M. Berngruber, L. Barbiero, E. Demler, N. Goldman, I. Bloch, and M. Aidelsburger, *Nat. Phys.* **15**, 1168 (2019).
- [46] A. Mil, T. V. Zache, A. Hegde, A. Xia, R. P. Bhatt, M. K. Oberthaler, P. Hauke, J. Berges, and F. Jendrzejewski, *Science* **367**, 1128 (2020), <https://science.sciencemag.org/content/367/6482/1128.full.pdf>
- [47] B. Yang, H. Sun, R. Ott, H.-Y. Wang, T. V. Zache, J. C. Halimeh, Z.-S. Yuan, P. Hauke, and J.-W. Pan, *Nature* **587**, 392 (2020).
- [48] N. Klco, E. F. Dumitrescu, A. J. McCaskey, T. D. Morris, R. C. Pooser, M. Sanz, E. Solano, P. Lougovski, and M. J. Savage, *Phys. Rev. A* **98**, 032331 (2018).
- [49] H. Lamm, S. Lawrence, and Y. Yamauchi (NuQS Collaboration), *Phys. Rev. D* **100**, 034518 (2019).
- [50] N. Klco, M. J. Savage, and J. R. Stryker, *Phys. Rev. D* **101**, 074512 (2020).
- [51] D. Paulson, L. Dellantonio, J. F. Haase, A. Celi, A. Kan, A. Jena, C. Kokail, R. van Bijnen, K. Jansen, P. Zoller, and C. A. Muschik, “Towards simulating 2d effects in lattice gauge theories on a quantum computer,” (2020), [arXiv:2008.09252](https://arxiv.org/abs/2008.09252) [quant-ph].
- [52] A. Ciavarella, N. Klco, and M. J. Savage, *Phys. Rev. D* **103**, 094501 (2021).
- [53] Y. Atas, J. Zhang, R. Lewis, A. Jahanpour, J. F. Haase, and C. A. Muschik, “Su(2) hadrons on a quantum computer,” (2021), [arXiv:2102.08920](https://arxiv.org/abs/2102.08920) [quant-ph].
- [54] E. Zohar, “Quantum simulation of lattice gauge theories in more than one space dimension – requirements, challenges, methods,” (2021), [arXiv:2106.04609](https://arxiv.org/abs/2106.04609) [quant-ph].
- [55] J. Kogut and L. Susskind, *Physical Review D* **11**, 395 (1975).
- [56] H. Weimer, M. Muller, I. Lesanovsky, P. Zoller, and H. P. Büchler, *Nat Phys* **6**, 382 (2010).
- [57] E. Shahmoon and G. Kurizki, *Phys. Rev. A* **87**, 33831 (2013).
- [58] J. S. Douglas, H. Habibian, C.-L. Hung, A. V. Gorshkov, H. J. Kimble, and D. E. Chang, *Nat. Photon.* **9**, 326 (2015).
- [59] A. González-Tudela, E. Del Valle, and F. Laussy, *Phys. Rev. A* **91** (2015), [10.1103/PhysRevA.91.043807](https://doi.org/10.1103/PhysRevA.91.043807).
- [60] C.-L. Hung, A. González-Tudela, J. Ignacio Cirac, and H. Kimble, *Proc. Natl. Acad. Sci. U.S.A.* **113** (2016), [10.1073/pnas.1603777113](https://doi.org/10.1073/pnas.1603777113).
- [61] A. Goban, C.-L. Hung, S.-P. Yu, J. D. Hood, J. A. Muniz, J. H. Lee, M. J. Martin, A. C. McClung, K. S. Choi, D. E. Chang, O. Painter, and H. J. Kimble, *Nat. Commun.* **5**, 3808 (2014).
- [62] J. D. Thompson, T. G. Tiecke, N. P. de Leon, J. Feist, A. V. Akimov, M. Gullans, A. S. Zibrov, V. Vuletić, and M. D. Lukin, *Science* **340**, 1202 (2013).
- [63] T. G. Tiecke, J. D. Thompson, N. P. de Leon, L. R. Liu, V. Vuletić, and M. D. Lukin, *Nature* **508**, 241 (2014).
- [64] A. Goban, C.-L. Hung, J. D. Hood, S.-P. Yu, J. A. Muniz, O. Painter, and H. J. Kimble, *Phys. Rev. Lett.* **115**, 63601 (2015).
- [65] J. D. Hood, A. Goban, A. Asenjo-Garcia, M. Lu, S.-P. Yu, D. E. Chang, and H. J. Kimble, *Proc. Natl. Acad. Sci. U.S.A.* **113**, 10507 (2016).
- [66] M. E. Kim, T. H. Chang, B. M. Fields, C. A. Chen, and C. L. Hung, *Nature Communications* (2019), [10.1038/s41467-019-09635-7](https://doi.org/10.1038/s41467-019-09635-7).
- [67] X. Luan, J. Béguin, A. P. Burgers, Z. Qin, S. Yu, and H. J. Kimble, *Advanced Quantum Technologies* (2020), [10.1002/qute.202000008](https://doi.org/10.1002/qute.202000008).
- [68] J.-B. Béguin, J. Laurat, X. Luan, A. P. Burgers, Z. Qin, and H. J. Kimble, *Proc. Natl. Acad. Sci. U.S.A.* **117**, 202014017 (2020).
- [69] T.-H. Chang, B. M. Fields, M. E. Kim, and C.-L. Hung, *Optica* **6**, 1203 (2019).
- [70] T. Dordevic, P. Samutpraphoot, P. L. Ocola, H. Bernien, B. Grinkemeyer, I. Dimitrova, V. Vuletić, and M. D. Lukin, “Nanophotonic quantum interface and transportable entanglement for atom arrays,” (2021), [arXiv:2105.06485](https://arxiv.org/abs/2105.06485) [quant-ph].
- [71] H. Ritsch, P. Domokos, F. Brennecke, and T. Esslinger, *Rev. Mod. Phys.* **85**, 553 (2013).
- [72] E. J. Davis, G. Bentsen, L. Homeier, T. Li, and M. H. Schleier-Smith, *Phys. Rev. Lett.* **122**, 010405 (2019).
- [73] G. Bentsen, T. Hashizume, A. S. Buyskikh, E. J. Davis, A. J. Daley, S. S. Gubser, and M. Schleier-Smith, *Phys. Rev. Lett.* **123**, 130601 (2019).
- [74] A. Periwal, E. S. Cooper, P. Kunkel, J. F. Wienand, E. J. Davis, and M. Schleier-Smith, “Programmable interactions and emergent geometry in an atomic array,” (2021), [arXiv:2106.04070](https://arxiv.org/abs/2106.04070) [quant-ph].
- [75] L. Tagliacozzo, A. Celi, A. Zamora, and M. Lewenstein, *Annals of Physics* **330**, 160 (2013).
- [76] D. Horn, M. Weinstein, and S. Yankielowicz, *Physical Review D* **19**, 3715 (1979).
- [77] G. 't Hooft, *Nuclear Physics B* **138**, 1 (1978).
- [78] F. J. Wegner, *Journal of Mathematical Physics* **12**, 2259 (1971), <https://doi.org/10.1063/1.1665530>.
- [79] S. Notarnicola, E. Ercolessi, P. Facchi, G. Marmo, S. Pascazio, and F. V. Pepe, *J. Phys. A: Math. Theor.* **48**, 30FT01 (2015).
- [80] L. Barbiero, C. Schweizer, M. Aidelsburger, E. Demler, N. Goldman, and F. Grusdt, *Science Advances* **5** (2019), [10.1126/sciadv.aav7444](https://doi.org/10.1126/sciadv.aav7444), <https://advances.sciencemag.org/content/5/10/eaav7444.full.pdf>.
- [81] X. Cui, Y. Shi, and J. Yang, *J. High Energ. Phys.* **2020**, 160 (2020).
- [82] L. Homeier, C. Schweizer, M. Aidelsburger, A. Fedorov, and F. Grusdt, “ \mathbb{Z}_2 lattice gauge theories and kitaev’s toric code: A scheme for analog quantum simulation,” (2020), [arXiv:2012.05235](https://arxiv.org/abs/2012.05235) [quant-ph].
- [83] D. González-Cuadra, L. Tagliacozzo, M. Lewenstein, and A. Bermudez, *Phys. Rev. X* **10**, 041007 (2020).
- [84] E. J. Gustafson and H. Lamm, *Phys. Rev. D* **103**, 054507 (2021).
- [85] H. F. Trotter, *Proceedings of the American Mathematical Society* **10**, 545 (1959).
- [86] M. Suzuki, *Journal of Mathematical Physics* **26**, 601 (1985).
- [87] B. Reznik, Y. Aharonov, and B. Groisman, *Phys. Rev. A* **65**, 8 (2002).
- [88] E. Zohar, *Journal of Physics A: Mathematical and Theoretical* **50**, 085301 (2017).
- [89] M. Heyl, P. Hauke, and P. Zoller, *Science Advances* **5**, eaau8342 (2019).
- [90] I. Bloch, J. Dalibard, and W. Zwerger, *Rev. Mod. Phys.* **80**, 885 (2008).
- [91] M. Endres, H. Bernien, A. Keesling, H. Levine, E. R. Anschuetz, A. Krajenbrink, C. Senko, V. Vuletić, M. Greiner, and M. D. Lukin, *Science* **354**, 1024 (2016).

- [92] D. Barredo, S. De Léséleuc, V. Lienhard, T. Lahaye, and A. Browaeys, *Science* **354**, 1021 (2016).
- [93] D. Barredo, V. Lienhard, S. De Léséleuc, T. Lahaye, and A. Browaeys, *Nature* **561**, 79 (2018).
- [94] W. S. Bakr, J. I. Gillen, A. Peng, S. Fölling, and M. Greiner, *Nature* **462**, 74 (2009).
- [95] J. F. Sherson, C. Weitenberg, M. Endres, M. Cheneau, I. Bloch, and S. Kuhr, *Nature* **467**, 68 (2010).
- [96] C. Weitenberg, M. Endres, J. F. Sherson, M. Cheneau, P. Schauß, T. Fukuhara, I. Bloch, and S. Kuhr, *Nature* **471**, 319 (2011).
- [97] A. González-Tudela, C.-L. Hung, D. Chang, J. Cirac, and H. Kimble, *Nat. Photon.* **9** (2015), 10.1038/nphoton.2015.54.
- [98] M. Suzuki, *J. Math. Phys.* **32**, 400 (1991).
- [99] E. Fradkin and S. H. Shenker, *Phys. Rev. D* **19**, 3682 (1979).
- [100] H. Rieger and N. Kawashima, *Eur. Phys. J. B* **9**, 233 (1999).
- [101] H. W. J. Blöte and Y. Deng, *Phys. Rev. E* **66**, 066110 (2002).
- [102] R. N. C. Pfeifer, G. Evenbly, and G. Vidal, *Phys. Rev. A* **79**, 040301 (2009).
- [103] A. Kitaev, *Annals of Physics* **303**, 2 (2003).
- [104] E. Zohar, *Phys. Rev. D* **101**, 034518 (2020).
- [105] G. Auletta, G. Parisi, and M. Fortunato, *Quantum Mechanics*. (Cambridge University Press, 2009) pp. 369–371.
- [106] A. González-Tudela, C.-L. Hung, D. E. Chang, J. I. Cirac, and H. J. Kimble, *Nature Photonics* **9**, 320 (2015).